2-30

Bulk Microphysical Properties of Orographic Rainfall Deduced by Vertically Pointing Radars in the Western United States

Allen B. White[1] (allen.b.white@noaa.gov), Daniel J. Gottas[1], Robert Cifelli[1], and Haonan Chen[2,1]

[1]NOAA Earth System Research Laboratory, Boulder, Colorado USA; [2]Cooperative Institute for Research in the Atmosphere, Colorado State University, Fort Collins, Colorado USA

I. INTRODUCTION

NOAA's Earth System Research Laboratory (ESRL) operates two different types of vertically pointing S-band Doppler radars: a pulsed radar (S-PROF; **Figure 1**; White et al. 2000) and a frequency-modulated, continuous-wave radar (SLR; **Figure 2**; Johnston et al. 2017). These radars provide vertical profiles of radar reflectivity and Doppler vertical velocity, which are subsequently analyzed to partition rainfall observed at the radar site into three categories using the technique developed by White et al. (2003): brightband (BB) rain, non-brightband (NBB) rain, and convective rain. NBB rain is primarily a shallow, warm rain process driven by collision and coalescence. Because of its shallow nature, NBB rain is often undetected by the operational U.S. WSR-88D precipitation scanning radar network, especially in the western U.S., where radar coverage is poorest. Examples of data collected by the S-PROF and SRL are shown in **Figures 3 and 4**, respectively.

II. RAINFALL PROCESS PARTITIONING METHODOLOGY

(1) Each radar profile is examined for the existence of a radar brightband.

(2) Statistics are computed for each 30-minute observation period that received at least 0.5 mm of rain. If less than 50% of the profiles identified as rain contain a bright band, then the period is assigned to nonbrightband (NBB) rain. If greater than or equal to 50% of the profiles contain a bright band, then the period is assigned to brightband (BB) rain.

(3) Periods labeled as NBB rain are inspected to subjectively determine if the algorithm was fooled by a) **convection**: the brightband structure is smeared by turbulent motions; b) **snow**: the brightband is below the minimum detectable radar range; or c) **attenuation**: wet snow has accumulated on the antenna radome preventing accurate reflectivity retrievals. With the SLR this problem is solved by using the sloped radomes.

(4) Algorithm results are modified accordingly and daily and seasonal statistics are produced (see **Table 1**)

Figure 1. The NOAA S-band precipitation profiling Doppler radar (S-PROF) at Santa Rosa, California (STR; see map). The shelter houses the radar hardware and data communications computer. An example of S-PROF data is shown in **Figure 3**.

Figure 2. The NOAA S-band frequency-modulated, continuous-wave Doppler radar (SLR) at San Bernardino, California (SBO; see map). The shelter houses the radar hardware and data communications computer. An example of SRL data is shown in **Figure 4**.

Table 1. The annual wet-season percentage (by amount) of NBB rain sampled at S-PROF and SLR locations shown in **Figure 5**.

Water Year	S-band Pulsed Doppler Radars (S-PROF)										S-band FM-CW Doppler Radars (SLR)									
	CZC	DVS	HOP	MDT	MPI	SPD	STR	TCI	TDE	WPT	CFF	HCP	KNV	NER	OVL	PFD	SBO	SLR	STD	STH
1998	29.4																			
2001	18.2																			
2002	50.0																			
2003	41.5																			
2004	42.2																			
2005	29.3																			
2006	37.3																			
2007	38.0																			
2008	29.0																			
2009	31.6					38.8														
2010	26.4				14.1	32.8				15.6									7.7	
2011	30.6				16.0	27.2				13.1										
2012	24.9	8.0				14.8	18.6			17.5										
2013	21.3	15.3				21.2	26.8			11.4	29.1	13.6	28.7		14.7	23.1			19.3	
2014	33.2						20.4				20.2	9.0	9.6		12.1	8.4	58.9	7.7	19.0	
2015	25.5			22.3			22.9				19.6	11.5	11.5	13.5	13.7	11.8	35.5	17.3	16.4	19.0
2016	36.1		21.3	47.6			34.0		4.6		22.1	4.1	4.1	15.6	14.8	10.8	46.2	6.2	14.3	26.4
2017	31.2		21.7	39.4			32.2		6.6		23.0	3.9	3.9	17.6	19.9	16.1	43.1	18.3	20.5	25.5
2018	48.2		27.9	48.7			41.3	22.4			32.1	5.9	3.9	22.0	21.6	15.7	42.0	15.1	16.6	30.4
Avg.	**32.8**	**15.7**	**23.6**	**39.5**	**15.1**	**27.0**	**28.0**	**22.4**	**5.6**	**14.4**	**24.3**	**8.0**	**10.3**	**17.2**	**16.1**	**14.3**	**45.1**	**12.9**	**16.3**	**25.3**

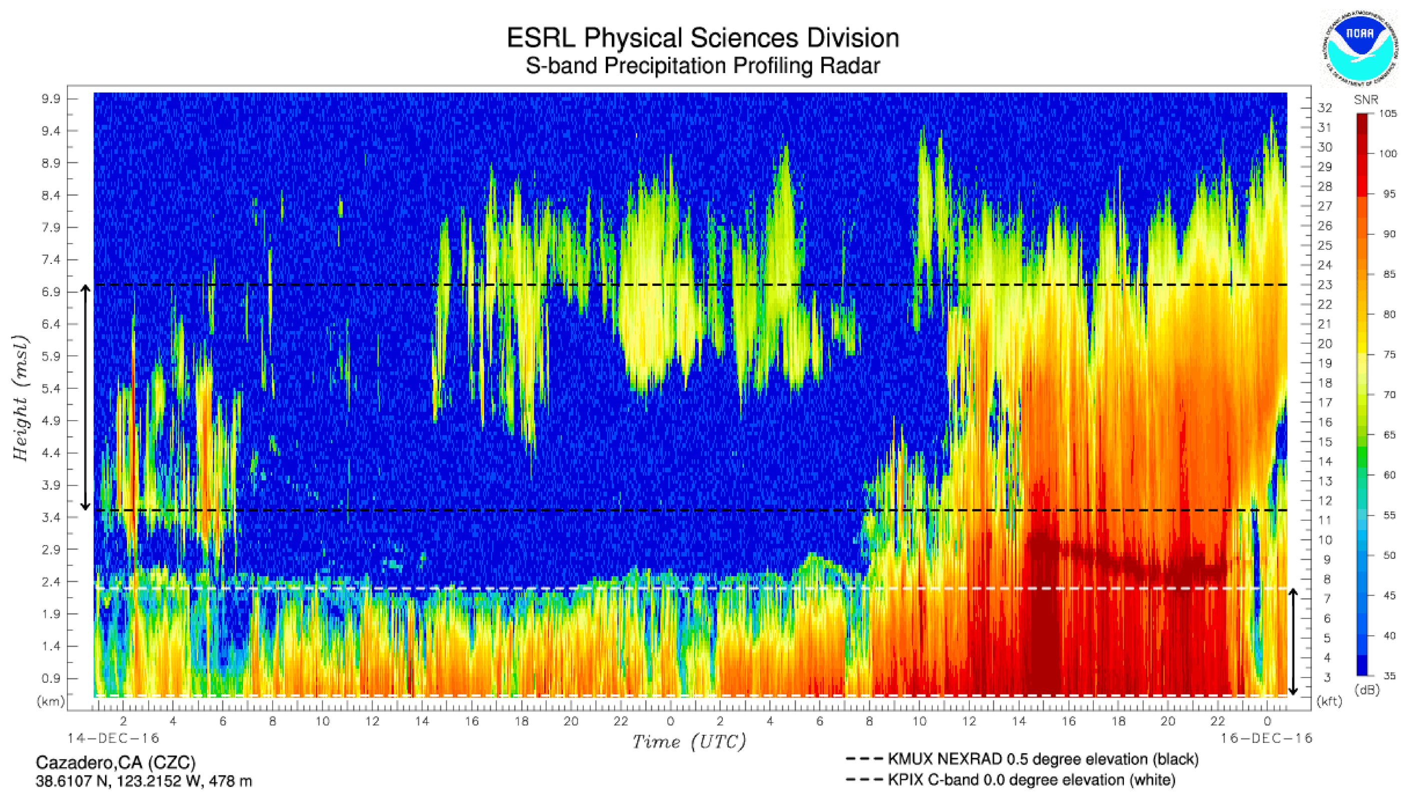

Figure 3. Time-height cross section of radar reflectivity in the form of range-corrected signal-to-noise ratio from the S-PROF at Cazadero, California (CZC; see map). The horizontal lines denote the beamwidth of two precipitation scanning radars.

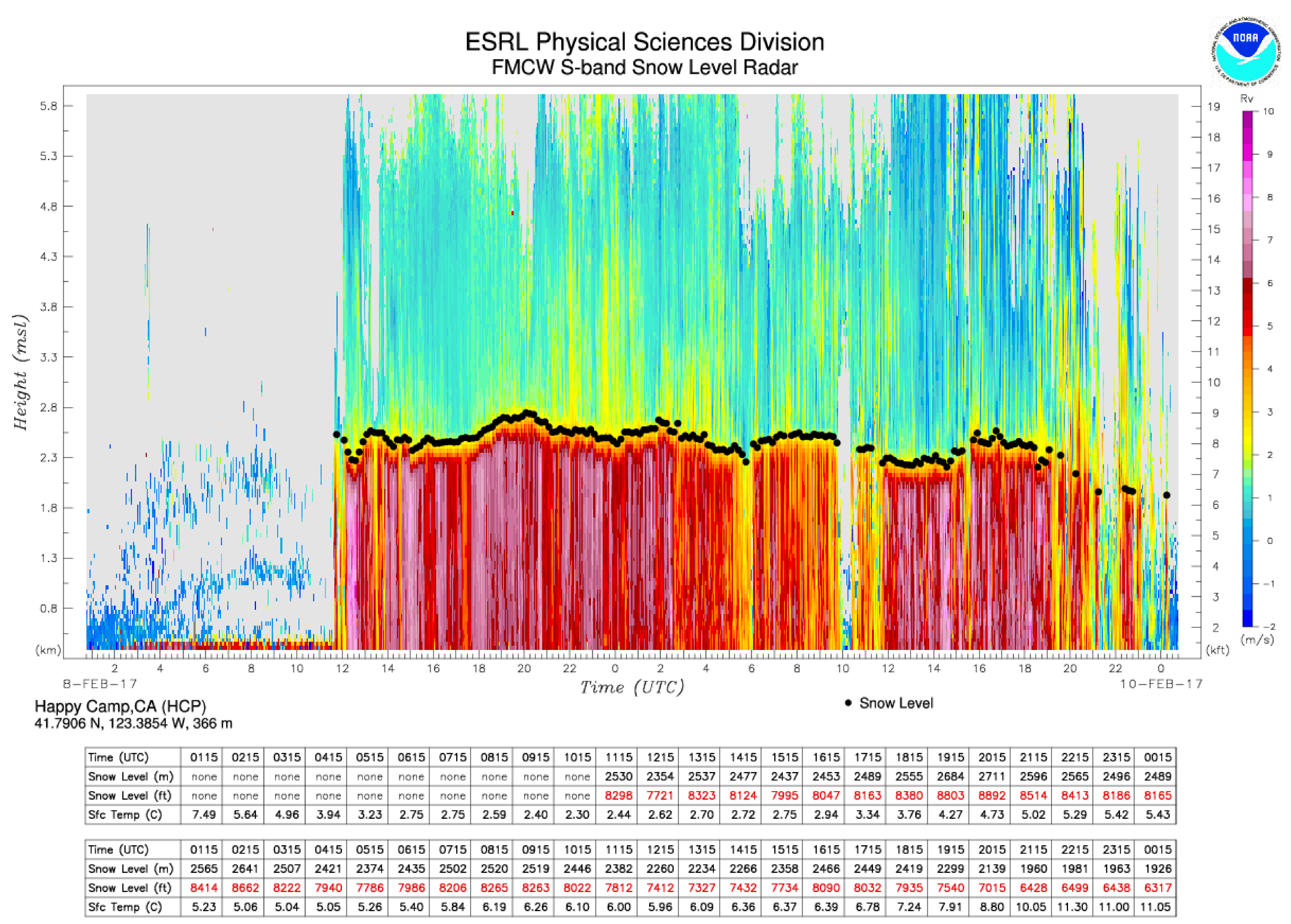

Figure 4. Time-height cross section of Doppler vertical velocity (Rv) from the SLR at Happy Camp, California (HCP; see map). The bright-band height (a.k.a. snow level) is denoted by the black dots. 30-min averages of the snow level and surface temperature are tabulated.

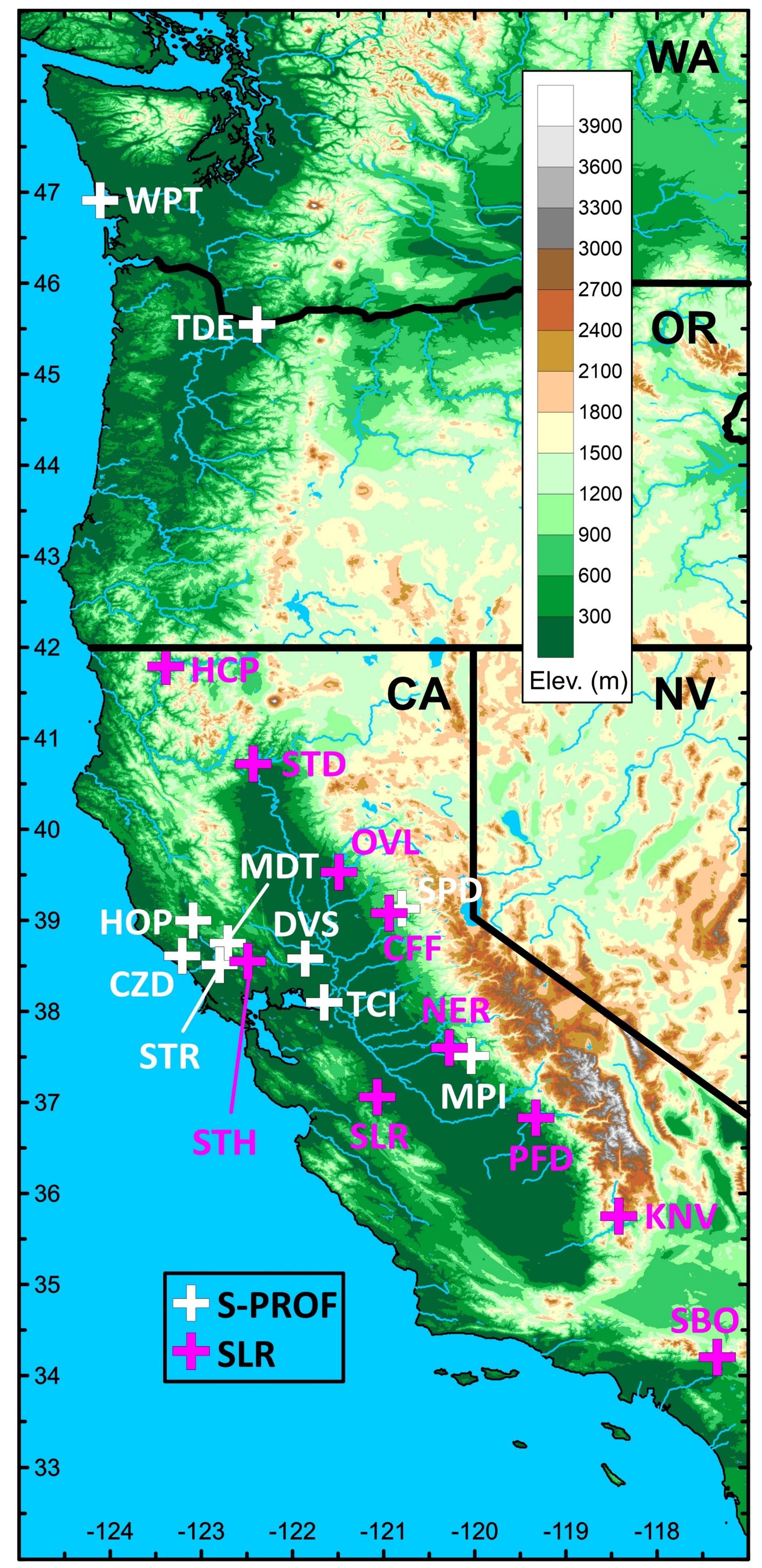

Figure 5. Terrain map of Western United States indicating the locations of S-PROF (white) and SLR (pink) radars listed in **Table 1**.

III. RESULTS

Figure 5 shows the locations where S-PROFs and SLRs have been deployed as part of NOAA's Hydrometeorology Testbed (HMT; hmt.noaa.gov) and other related projects. **Figure 6** compares BB and NBB rain observed at the MDT S-PROF site with rainfall estimated by NOAA's operational multi-radar, multi-sensor (MRMS) quantitative precipitation product. **Figure 7** illustrates differences in drop-size distribution parameters for BB and NBB rain (Martner et al. 2008).

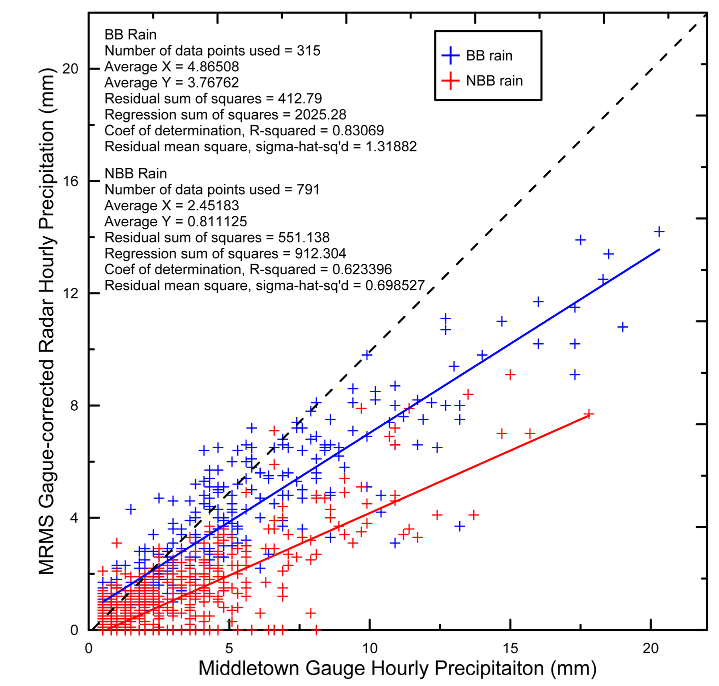

Figure 6. Scatterplots of gauge-measured rainfall versus rainfall estimated by gauge-corrected MRMS for BB (blue) and NBB (red) precipitation. Each point is a one-hour sample where at least 80% of the radar profiles were classified as either BB or NBB. One-to-one correlation is shown by the dashed line and lines of linear regression and statistics are given for each rainfall type. Data were collected December 2015 through May 2018.

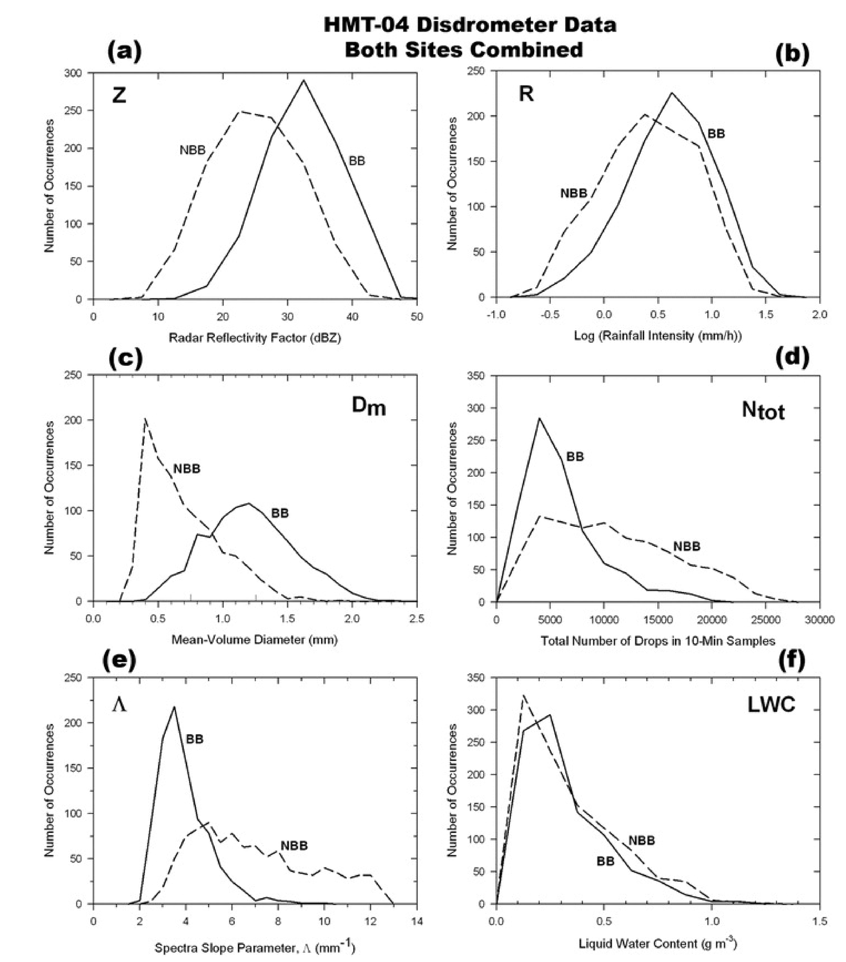

Figure 7. Frequency distributions of (a) reflectivity, (b) rainfall intensity, (c) mean-volume diameter, (d) total number of drops, (e) slope of the drop size spectrum, and (f) liquid water content derived from disdrometer 10-minute samples. From Martner et al. (2008).

IV. RELATED WORK

NOAA's ESRL, Colorado Sate University, U.S. Geological Survey (USGS), and Scripps Institution of Oceanography are partnering with water agencies in the San Francisco Bay area on the Advanced Quantitative Precipitation Information (AQPI) project. The project is sponsored by the California Department of Water Resources and is managed locally by Sonoma Water. The project will deploy five gap-filling radars such as the one shown below to improve quantitative precipitation estimation for this highly populated region. The project will also provide high resolution (1-km grid) precipitation forecasts from NOAA's High-Resolution Rapid-Refresh (HRRR) numerical weather prediction model. NOAA's National Water Model will be coupled to the coastal storm model (CoSMoS) developed by the USGS for coastal flood and inundation forecasts for the San Francisco Bay coastline.

V. REFERENCES

Johnston, P. E., J. R. Jordan, A. B. White, D. A. Carter, D. M. Costa, and T. E. Ayers, 2017: The NOAA FM-CW snow-level radar. *J. Atmos. Oceanic Technol.*, **34**, 247–267.

Martner, B. E., S. E. Yuter, A. B. White, S. Y. Matrosov, D. E. Kingsmill, and F. M. Ralph, 2008: Raindrop size distributions and rain characteristics in California coastal rainfall for periods with and without a radar bright band. *J. Hydrometeor.*, **9**, 408–425.

White, A. B., J. R. Jordan, B. E. Martner, F. M. Ralph, and B. W. Bartram, 2000: Extending the dynamic range of an S-band radar for cloud and precipitation studies. *J. Atmos. Oceanic Technol.*, **17**, 1226–1234.

White, A. B., P. J. Neiman, F. M. Ralph, D. E. Kingsmill, and P. O. G. Persson, 2003: Coastal orographic rainfall processes observed by radar during the California Land-Falling Jets Experiment. *J. Hydrometeor.*, **4**, 264–282.